Lesion Size Detection in Geographic Atrophy by Polarization-Sensitive Optical Coherence Tomography and Correlation to Conventional Imaging Techniques

Christopher Schütze,[1] *Matthias Bolz,*[1] *Ramzi Sayegh,*[1] *Bernhard Baumann,*[2] *Michael Pircher,*[2] *Erich Götzinger,*[2] *Christoph K. Hitzenberger,*[2] *and Ursula Schmidt-Erfurth*[1]

Purpose. To investigate the reproducibility of automated lesion size detection in patients with geographic atrophy (GA) using polarization-sensitive spectral-domain optical coherence tomography (PS-OCT) and to compare findings with scanning laser ophthalmoscopy (SLO), fundus autofluorescence (FAF), and intensity-based spectral-domain OCT (SD-OCT).

Methods. Twenty-nine eyes of 22 patients with GA were examined by PS-OCT, selectively identifying the retinal pigment epithelium (RPE). A novel segmentation algorithm was applied, automatically detecting and quantifying areas of RPE atrophy. The reproducibility of the algorithm was assessed, and lesion sizes were correlated with manually delineated SLO, FAF, and intensity-based SD-OCT images to validate the clinical applicability of PS-OCT in GA evaluation.

Results. Mean GA lesion size of all patients was 5.28 mm^2 (SD: 4.92) in PS-OCT. Mean variability of individual repeatability measurements was 0.83 mm^2 (minimum: 0.05; maximum: 3.65). Mean coefficient of variation was 0.07 (min: 0.01; max: 0.19). Mean GA area in SLO (Spectralis OCT) was 5.15 mm^2 (SD: 4.72) and 2.5% smaller than in PS-OCT ($P = 0.9$, Pearson correlation coefficient = 0.98, $P < 0.01$). Mean GA area in intensity-based SD-OCT pseudo-SLO images (Cirrus OCT) was 5.14 mm^2 (SD: 4.67) and 2.7% smaller than in PS-OCT ($P = 0.9$, Pearson correlation coefficient = 0.98, $P < 0.01$). Mean GA area of all eyes measured 5.41 mm^2 (SD: 4.75) in FAF, deviating by 2.4% from PS-OCT results ($P = 0.89$, Pearson correlation coefficient = 0.99, $P < 0.01$).

Conclusions. PS-OCT demonstrated high reproducibility of GA lesion size determination. Results correlated well with SLO, FAF, and intensity-based SD-OCT fundus imaging. PS-OCT may therefore be a valuable and specific imaging modality for automated GA lesion size determination in scientific studies and clinical practice. (*Invest Ophthalmol Vis Sci.* 2013;54:739–745) DOI:10.1167/iovs.11-7877

Age-related macular degeneration (AMD) is a neurodegenerative disease and the most frequent cause of severe visual loss among older individuals in industrialized populations.[1–4] The determining characteristic of the condition is an alteration of the retinal pigment epithelium (RPE) layer, manifesting with drusen, related to early to intermediate AMD. Advanced stages of AMD include geographic atrophy (GA) and choroidal neovascularization (CNV). GA (also called advanced "dry" AMD) causes substantial and progressive visual impairment,[5] developing in 20% of patients presenting with preexisting clinical signs of AMD.[1,6–8] The disease is characterized by confluent areas of apoptosis at the level of photoreceptors and RPE atrophy, occurring bilaterally in more than half of patients affected,[9–11] confirmed by histopathological studies.[12] The condition progresses slowly over time, sparing the fovea until late during the course of the disease.[12–16] Prior to GA development, large drusen formation and the development of pigmentary changes, followed by fading of drusen, may occur.[17,18] As the dry form of AMD progresses only slowly, research has primarily focused on the pathomechanism of CNV with its dramatic course, and less attention has been paid to GA. Moreover, to date, no proven treatment strategy is available to halt or decelerate GA disease progression.[19]

Due to the increasing prevalence of GA and the substantial risk of progressive visual impairment, intensive efforts have been undertaken with regard to a better understanding of the underlying pathophysiology of the disease. As the atrophic lesion is the hallmark of the disease, early diagnosis and exact assessment of GA lesion dimensions and growth rates are fundamental. Several diagnostic modalities, such as scanning laser ophthalmoscopy (SLO), fundus autofluorescence (FAF), and spectral-domain (SD) optical coherence tomography (OCT), have been suggested for in vivo visualization and quantification of GA.[20–24]

Recently, polarization-sensitive OCT (PS-OCT)[25–30,31,32] has been introduced, providing selective identification of the RPE layer based on tissue-specific polarizing properties.[25–30] In order to obtain polarization-specific information, the retina is scanned by a light beam of a defined polarization state that is detected and analyzed by a polarization-sensitive detection unit. Since the human retina contains structures with distinct polarization-preserving (e.g., photoreceptor layer), birefringent (e.g., retinal nerve fiber layer), or depolarizing properties (RPE), PS-OCT can be used to differentiate retinal tissues based on their specific polarization contrast. These layers can be precisely distinguished based on the characteristic interaction with the incident illumination.[25–30] The detection and seg-

From the [1]Department of Ophthalmology, Medical University of Vienna, Vienna, Austria; and the [2]Center for Medical Physics and Biomedical Engineering, Medical University of Vienna, Vienna, Austria.

Supported by an independent scientific grant (FWF Grant P19624-B02, Austrian Science Fund) and the European Union (FP7 HEALTH Program Grant 201880, FUN-OCT).

Submitted for publication May 14, 2011; revised January 21, July 7, October 25, and December 8, 2012; accepted December 11, 2012.

Disclosure: **C. Schütze**, None; **M. Bolz**, None; **R. Sayegh**, None; **B. Baumann**, Canon (F); **M. Pircher**, Canon (F); **E. Götzinger**, Canon (F); **C.K. Hitzenberger**, Canon (F); **U. Schmidt-Erfurth**, None

Corresponding author: Ursula Schmidt-Erfurth, Department of Ophthalmology, Medical University of Vienna, Waehringer Guertel 18-20, 1090 Vienna, Austria;
ursula.schmidt-erfurth@meduniwien.ac.at

Copyright 2013 The Association for Research in Vision and Ophthalmology, Inc.

Downloaded from iovs.arvojournals.org on 05/07/2021

mentation of the RPE by PS-OCT are based on the polarization-scrambling properties of this layer, providing a method ideally suitable to image any GA lesion present.

Our group[30] has recently developed a novel segmentation algorithm capable of automatically detecting and quantifying atrophic areas based on the depolarizing property of the RPE. The algorithm was tested in a small number of patients with GA,[30] with an average coefficient of variation of 0.092. It was the aim of this study to evaluate the reproducibility of automated lesion size detection using PS-OCT in a greater patient cohort, as well as to compare the novel method with conventional techniques such as SLO, FAF, and SD-OCT–based fundus (pseudo-SLO) imaging in order to determine its potential clinical value.

Methods

Twenty-nine eyes of 22 patients diagnosed with GA were included in this prospective cross-sectional trial. The mean age of patients included was 77 years (SD: 8.15; min: 59; max: 91); 10 patients were female, and 12 were male. Thirteen right eyes and 16 left eyes were included. Mean best corrected visual acuity (BCVA) was 0.42 Snellen (SD: 0.35; min: 0.05; max: 1.0). The protocol as well as possible consequences of the study procedures were explained in detail prior to patient inclusion. Written informed consent was obtained from each patient. The study protocol was approved by the local ethics committee and adhered to the ethical tenets of the Declaration of Helsinki.

Exclusion criteria were the presence of other confounding retinal pathologies, including neovascular AMD, macular dystrophies, and macular scars; these were excluded by medical history and fluorescein angiography following a standardized procedure.

All patients underwent a comprehensive ophthalmologic examination, including BCVA and slit-lamp biomicroscopy, as well as fundus photography, PS-OCT, and SD-OCT measurements after pupil dilation with Tropicamid 0.5% and phenylephrine 2.5% at a single visit.

In the current study, all patients were affected by one central GA lesion; four of these patients revealed multifocal GA. In addition to the quantitative reproducibility analysis of the central GA lesion present, a preliminary evaluation with respect to lesion size repeatability in eyes with multifocal GA by PS-OCT was carried out. Further, a correlation analysis of GA lesions to FAF, SLO, and pseudo-SLO was performed. No patient included in this study showed foveal sparing.

The reproducibility of automated GA lesion size evaluation by PS-OCT was assessed in each eye by comparing the size of RPE atrophy in a set of five individual measurements. Further, GA dimensions evaluated by the novel PS-OCT algorithm were compared with lesion dimensions identified in SLO, FAF, and intensity-based pseudo-SLO images in order to assess clinical validity.

Imaging Procedures and Properties of Imaging Devices

A PS-OCT prototype developed by the Center for Medical Physics and Biomedical Engineering, Medical University of Vienna, capable of measuring multiple biophysical parameters simultaneously (reflectivity, retardation, optic axis orientation, degree of polarization uniformity [DOPU]),[29] was used to obtain images of posterior pole layers, including the RPE layer and melanin-containing structures at the choroidal level. Details of the instrument have been published previously.[30] The instrument includes an additional channel for recording SLO images, which allows for acquisition of fast online fundus images. The SLO channel uses the same superluminescent diode as the OCT channel for retinal illumination, but a separate detector (avalanche diode) is used for alignment purposes. In OCT mode, the device records high-resolution 3-D PS-OCT datasets in 3.3 seconds at a raster scanning speed of 20,000 A-scans per second, with an axial resolution of 4.5 μm in tissue. Three different scanning patterns are available for 3-D imaging: 64×1024, 128×512, and 256×256. In this study the 128×512 pattern was used, imaging an area of 6.2×6.7 mm^2. Prior to calculation of polarization properties, pseudo-SLO images were generated by integrating the complete set of OCT intensity data in the A-scan direction for all A-scans, providing an en face overview of the imaged area. Although this is slower than the direct SLO channel, the pseudo-SLO images have the advantage of a perfect pixel-to-pixel correspondence to the OCT data. In a next step, the RPE is segmented based on its depolarizing property.

The algorithm used for RPE segmentation is based on Stokes vector analysis and has been described in detail elsewhere.[29,30] Stokes vector elements were derived from the PS-OCT data and averaged over adjacent pixels by calculating the mean value of each Stokes vector element within a rectangular window. Subsequently, DOPU (a quantity related to the classical degree of polarization) was calculated as a function of position. The RPE is characterized by depolarization of backscattered light, that is, by low values of DOPU, allowing for a selective differentiation of the RPE (Fig. 1J). To segment the RPE, we defined a threshold value of DOPU = 0.8. Pixels where DOPU was <0.8 were classified as depolarizing; consequently, special color values (red for pixels within the region of the RPE band, green for pixels below the RPE/Bruch's membrane complex; cf. Fig. 1I) were assigned to these pixels, thereby segmenting depolarizing tissue. The threshold value of 0.8 was found empirically to provide the best segmentation results for the imaging parameters used (raster scan pattern, averaging window size). The result of this procedure is an overlay image in which the segmented RPE is shown in red on top of the intensity image provided by the PS-OCT instrument while depolarizing pigmented areas within the choroid appear in green. This procedure enabled the visualization of overlying retinal layers together with the RPE layer with a precise topography and demarcation.

Segmentation of Geographic Atrophy Lesions

After segmentation of depolarizing tissue as described above, atrophic zones are detected and quantified by an algorithm described previously.[30] In brief, this algorithm sums the depolarizing pixels over each A-line of a segmented 3-D dataset, generating a thickness map of depolarizing tissue. Since the choroid may also contain depolarizing pigments shown in green (Fig. 1I), areas below the RPE/Bruch's membrane complex are excluded by the algorithm. To assess the extension of atrophic lesions, the thickness map is binarized and smoothed. In a last step, the algorithm automatically detects patches of connected pixels, which can be converted into atrophic areas by scaling them with the known pixel area (Fig. 1E). Retinal blood vessels can cast shadows and attenuate the OCT signal in the retina and RPE directly below the blood vessel. Beneath thick blood vessels, the RPE may appear atrophic along the shadow and thereby potentially add to the area appearing atrophic. However, no such shadowing artifacts were observed within the atrophic zones of the eyes included in this study.

GA lesions were detected fully automatically in the current study; however, if needed, the algorithm allows manual adjustments of segmentation parameters to account for differing scan quality. The same parameters were used for all datasets in this study.

FAF and infrared (IR) reflectance SLO imaging was performed by a Spectralis system (software version 4.0.0.0; Heidelberg Engineering, Heidelberg, Germany). The device is capable of combining FAF, SLO, IR, and SD-OCT, imaging an area of $\sim 9 \times 9$ mm^2. Intensity-based SD-OCT fundus imaging (pseudo-SLO imaging) was performed using Cirrus OCT (Cirrus, Dublin, CA), covering an area of 6×6 mm^2.

Data Analysis

For evaluating the reproducibility of PS-OCT datasets, five individual measurements per eye were performed. On the one hand, the central GA region present in each patient was assessed in all patients as described above, accounting for a total of 29 GA regions. On the other hand, the reproducibility of multifocal GA quantification by PS-OCT was evaluated. Mean values of all measurements per eye, standard deviation (SD), and the coefficient of variation were calculated. Mean variability of all GA

Downloaded from iovs.arvojournals.org on 05/07/2021

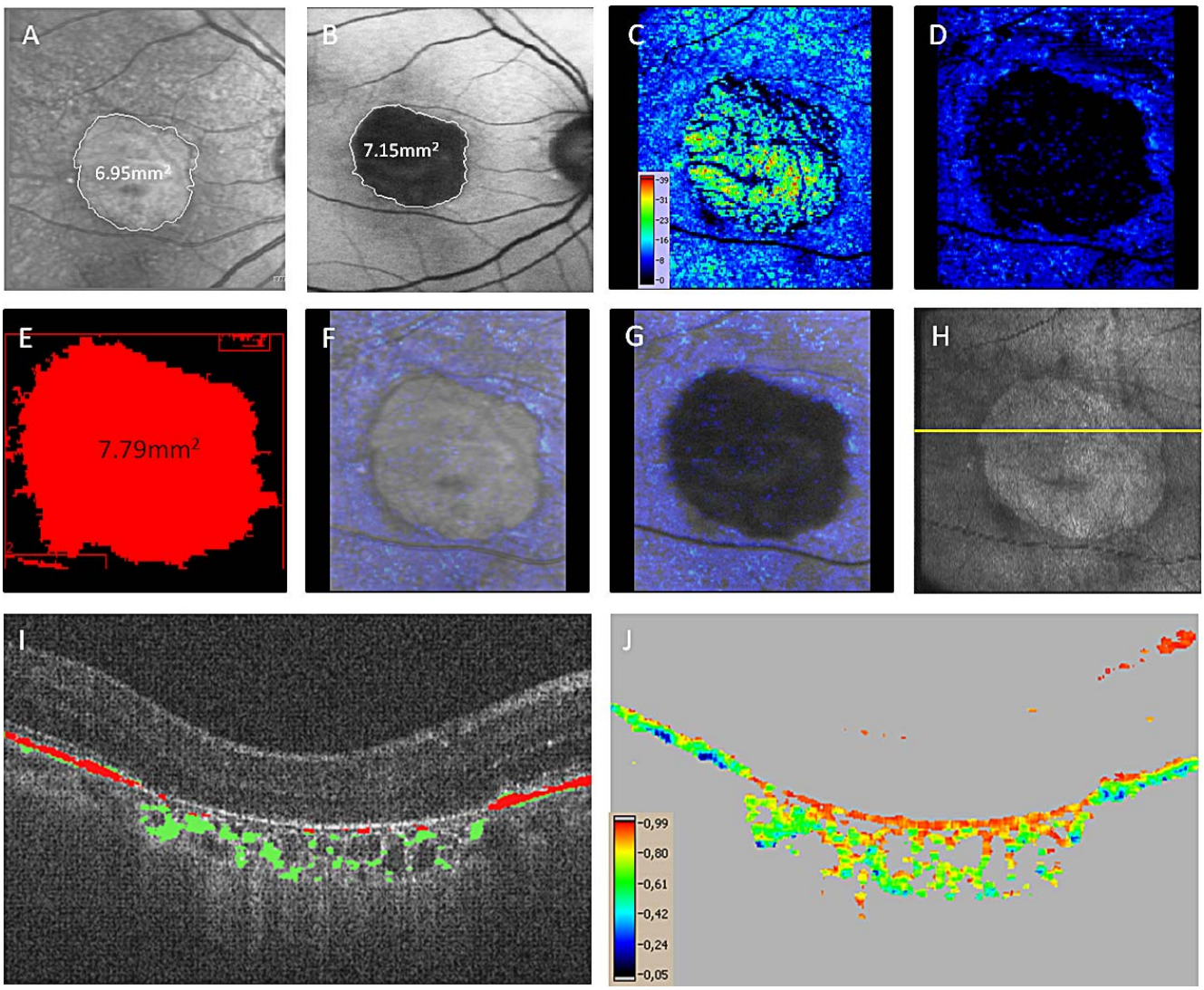

Figure 1. Sequence of images of a patient with geographic atrophy (GA) imaged by PS-OCT, autofluorescence (FAF), and scanning laser ophthalmoscopy (SLO). (**A**) shows a manually delineated GA lesion in an SLO image. (**B**) depicts the manually delineated FAF image. A thickness map of the overall depolarizing tissue generated by PS-OCT is represented in (**C**), while the thickness map in (**D**) exclusively includes depolarizing pixels originating from the RPE level, extracted by the segmentation algorithm. The automated RPE atrophy lesion quantified by PS-OCT (7.79 mm^2 in this eye) is shown in (**E**), based on automated detection and quantification (binary image). (**F**) Overlay of the PS-OCT and SLO images. (**G**) Overlay of the FAF and automatically delineated PS-OCT image. The SLO as well as the FAF images reveal an excellent topographic correlation with the automated RPE segmentation by PS-OCT. (**H**) provides an en face pseudo-SLO image; (**I**) illustrates an overlay of the morphology of the depolarizing layer (*red*: RPE level; *green*: choroid level) with the corresponding structural B-scan of the retina generated by PS-OCT. The degree of polarization uniformity (DOPU) image providing a selective identification of pigmented tissue due to inherent depolarizing properties is shown in (**J**).

lesion dimensions obtained from the PS-OCT repeatability measurements was assessed. Mean variability is the minimum lesion size value subtracted from the maximum value per patient, followed by calculation of the mean of all patients. In order to demonstrate the correlation of data acquired by PS-OCT with SLO, pseudo-SLO, and FAF values, correlation analyses and graphical representations (Pearson correlation coefficients and Bland–Altman plots) were used. Statistical software used was SPSS 15.0 (IBM SPSS, Armonk, NY) and Med Calc 11.5.1.0 (Med Calc, Ostend, Belgium). Further, the paired sample *t*-test was applied. Statistical significance was defined as $P < 0.05$.

Results

Twenty-two subjects (29 eyes) with GA were included in the current study. Each imaged eye was affected by at least one central GA lesion.

Mean size of GA lesions of all patients measured by PS-OCT was 5.28 mm^2 (SD: 4.92; min: 0.18; max: 17.03). Mean variability of all GA lesion dimensions verified from the repeatability measurements was 0.83 mm^2 (min: 0.05; max: 3.65). The coefficient of variation (SD/mean) was 0.07 on average (min: 0.01; max: 0.19). Table 1 summarizes the results. Multifocal GA was detected in four patients, each revealing two isolated GA lesions in PS-OCT. All multifocal RPE atrophy lesions were detected reproducibly by PS-OCT (mean: 2.60 mm^2; SD: 0.13; min: 2.6; max: 13.5). Although no patient included showed foveal sparing, residual areas of healthy RPE inside lesions of GA were detected in four patients and were identified reproducibly at identical locations in all cases by PS-OCT.

Figure 1 shows a representative example of the results of automated RPE atrophy detection and quantification by PS-

Downloaded from iovs.arvojournals.org on 05/07/2021

Table 1. Repeatability of the Automated PS-OCT Segmentation Algorithm in GA Evaluation

Patient No.	Mean Area*	Median Area*	SD*	Coefficient of Variation
1	8.14	8.32	0.36	0.04
2	0.55	0.56	0.03	0.06
3	1.64	1.65	0.03	0.02
4	3.50	3.61	0.25	0.07
5	7.90	7.84	0.16	0.02
6	4.99	4.94	0.19	0.04
7	6.96	6.85	0.29	0.04
8	7.56	7.57	0.08	0.01
9	0.18	0.18	0.03	0.16
10	4.49	4.54	0.20	0.04
11	0.41	0.41	0.08	0.19
12	14.87	14.86	0.61	0.04
13	15.26	15.25	1.60	0.10
14	1.25	1.29	0.17	0.14
15	4.20	4.27	0.43	0.10
16	1.1	1.08	0.08	0.07
17	8.86	8.96	0.28	0.03
18	1.04	0.99	0.16	0.16
19	2.68	2.77	0.20	0.07
20	4.16	4.08	0.30	0.07
21	0.96	0.96	0.08	0.08
22	1.37	1.36	0.11	0.08
23	6.22	6.30	0.33	0.05
24	17.03	17.38	1.19	0.06
25	0.37	0.37	0.02	0.05
26	5.31	5.30	0.57	0.11
27	2.22	2.2	0.19	0.08
28	13.61	13.66	0.72	0.05
29	6.29	6.26	0.67	0.11
Average	5.28	5.30	0.32	0.07
Min	0.18	0.18	0.18	0.01
Max	17.03	17.38	1.60	0.19

* Mean area and standard deviation of determined areas are given in mm^2.

OCT compared to manually delineated GA lesions in SLO and FAF images in a 67-year-old patient. Figure 1A shows a manually segmented GA area in an SLO image. Figure 1B reveals a manually bordered GA lesion in an FAF image. A map of the GA lesion generated by PS-OCT is shown, including an overall thickness map of the entire depolarizing tissue present throughout all layers, in Figure 1C. Figure 1D represents an automatically generated PS-OCT map of the same lesion, including only depolarizing pixels originating from the topographic RPE location (i.e., the red pixels in the segmented B-scan images [Fig. 1I]). Figure 1E displays the respective GA lesion detected and quantified by the PS-OCT software algorithm (binary image). After processing of this image as described earlier, a defined area of RPE atrophy measuring 7.79 mm^2 in size was automatically detected and quantified as illustrated (Fig. 1E). An overlay of the PS-OCT and SLO image (Figs. 1A, 1D) was performed as shown in Figure 1F, demonstrating a reliable topographic correlation. Figure 1G indicates an overlay of the PS-OCT and FAF image (Figs. 1B, 1D), revealing good topographic agreement. Figure 1H represents an en face pseudo-SLO image generated from the 3-D PS-OCT dataset (intensity data). Figure 1I demonstrates the B-scan corresponding to the yellow line in Figure 1H. Retinal layers are shown with depolarizing tissue color coded in an overlay. Detected depolarizing structures at the RPE level are represented in red; those from the choroid level are shown in green. The DOPU image reveals a specific identification of the RPE and choroidal pigments due to intrinsic depolarizing properties as shown in Figure 1J.

Table 2 summarizes the results of manually delineated SLO, FAF, and pseudo-SLO (Cirrus) images in comparison to automatically measured RPE atrophy lesions by PS-OCT (single eye comparison).

Mean size of RPE atrophy in SLO (by Spectralis) images was 5.15 mm^2 (SD: 4.72; min: 0.24; max: 16.3). SLO lesion size values were on average 0.13 mm^2 (2.5%) smaller than PS-OCT measurements, implying a good overall agreement in measured RPE atrophy size ($P = 0.9$). Pearson correlation coefficient was 0.98 with a significance of $P < 0.01$. Pseudo-SLO images acquired by Cirrus OCT had a mean GA lesion size of 5.14 mm^2 (SD: 4.67; min: 0.17; max: 16.25) and were only 0.14 mm^2 (2.7%) smaller in size when compared to average PS-OCT results ($P = 0.9$), indicating good agreement. Pearson correlation coefficient was $r = 0.98$ with $P < 0.01$. GA lesion dimensions measured by Spectralis SLO were smaller than mean PS-OCT results in 16 out of 27 cases (59%) and were smaller in 21 out of 27 cases (78%) in Cirrus pseudo-SLO images. Differences between PS-OCT, SLO, and pseudo-SLO results were not statistically significant ($P = 0.86$ for Spectralis and $P = 0.88$ for Cirrus OCT). Therefore, similar lesion size detection in SLO and PS-OCT imaging was apparent.

Measurements of GA lesions in FAF images revealed a mean size of 5.41 mm^2 (SD: 4.75; min: 0.24; max: 15.8). FAF values were on average 0.13 mm^2 (2.4%) larger than PS-OCT values. This result was statistically insignificant ($P = 0.89$). Pearson correlation coefficient was 0.99 with a significance of $P < 0.01$.

Overall, there was a high correlation of PS-OCT with all other imaging modalities (SLO, pseudo-SLO, and FAF) regarding GA lesion size determination.

Figure 2 represents Bland–Altman plots illustrating the results of PS-OCT, SLO, and FAF measurements. Pseudo-SLO results are not illustrated in Figure 2 due to high similarity and for reasons of space.

Discussion

The measurement of repeatability and the comparison with other modalities are important steps when one is implementing a new method. This study evaluated the reproducibility of automated lesion size detection in eyes with GA using PS-OCT and compared the results to conventional techniques such as SLO, pseudo-SLO, and FAF imaging.

Our results indicate good reproducibility of automated RPE atrophy detection by the PS-OCT software algorithm. Mean variability in measured GA areas as verified from our repeatability measurements, 0.83 mm^2, is considerably smaller than the progressive growth rate of 1.52 mm^2 per year and 4.57 mm^2 per 2 years during the natural history of the disease determined by FAF and fundus photography as reported in the literature.[19] In the current study, RPE lesion size measurements acquired by the automated PS-OCT software algorithm correlated well compared to SLO, pseudo-SLO, and FAF, with Pearson correlation coefficients of 099, 0.98, and 0.99, respectively ($P < 0.01$ in all cases). The deviations between PS-OCT and the other imaging modalities ranged between 2.4% and 2.7%. None of these differences was statistically significant. Moreover, preliminary analysis of the quantitative reproducibility of multifocal GA by PS-OCT showed good results in the current study. Further studies are needed to confirm the repeatability evaluation of multifocal GA in affected patients.

In comparison to SLO, intensity-based SD-OCT, or FAF (which images lipofuscin), the significant advantage of PS-OCT is that it measures the polarization contrast of backscattered

Downloaded from iovs.arvojournals.org on 05/07/2021

Table 2. Representation of the Results of GA Lesion Size Evaluation Obtained by PS-OCT Single Eye Measurements, FAF, and SLO

Patient No.	PS-OCT Single Scan*	FAF*	SLO (Spectralis)*	Pseudo-SLO (Cirrus)*
1	8.32	8.30	7.68	7.8
2	0.56	0.85	0.46	0.42
3	1.65	1.47	1.42	1.52
4	3.29	3.29	3.17	3.44
5	7.73	6.95	7.15	6.97
6	4.94	5.03	3.69	5.04
7	7.08	7.12	7.43	7.98
8	7.62	7.64	7.91	7.52
9	0.14	0.24	0.24	0.17
10	4.58	5.20	5.07	4.46
11	0.41	0.66	0.45	N/A
12	14.79	13.97	12.00	12.2
13	14.19	15.80	14.46	13.5
14	1.23	1.51	1.21	1.24
15	4.65	4.44	3.97	4.16
16	1.07	N/A	N/A	N/A
17	9.07	N/A	N/A	N/A
18	1.03	1.28	1.22	1.29
19	2.87	2.51	2.59	2.12
20	4.07	4.02	4.10	4.08
21	0.90	N/A	1.08	0.95
22	1.33	N/A	N/A	N/A
23	6.65	6.24	6.11	6.17
24	17.95	15,7	15.11	16.25
25	0.37	0.32	0.30	0.62
26	5.16	5.38	5.9	5.29
27	2.40	2.14	2.29	1.87
28	13.66	13.39	16.3	15.48
29	6.25	6.6	6.8	6.48
Mean	5.30	5.41	5.15	5.14
SD	4.85	4.75	4.72	4.67
Minimum difference relative to PS-OCT†		0	0.02	0.01
Maximum difference relative to PS-OCT†		2.25	2.84	2.59

There were no statistically significant differences between the measurements of PS-OCT and FAF ($P = 0.89$), PS-OCT and Spectralis SLO ($P = 0.9$), or Spectralis SLO and FAF ($P = 0.79$). Further, there was no statistically significant difference between PS-OCT results and Cirrus pseudo-SLO measurements ($P = 0.9$). Measurements were partly not analyzable in five patients (N/A) due to low scan quality. N/A, not available.

* Values are given in mm^2.

† Absolute values.

light. Thereby distinctive and unambiguous identification of the RPE is provided by an intrinsic, tissue-specific contrast mechanism. This property, together with the high correlation of results with those of other well-established imaging methods, makes PS-OCT potentially highly suitable for clinical evaluation of GA.

Several previous trials investigated the reproducibility of similar lesions in FAF/SLO imaging and showed conclusive results.[33,34] Schmitz-Valckenberg et al.[33] evaluated a method for automatically detecting and quantifying RPE atrophy in 24 eyes with GA using fundus FAF confocal SLO imaging. In that study, two independent readers analyzed GA areas manually by outlining them using a mouse-driven arrow (method A) and automatically using image analysis software (Global Lab Image/2) following subjective adjustment of thresholding (method B). Subsequently, agreement between methods A and B was assessed. The mean difference between readers was 0.39 mm^2 (95% confidence interval = CI [0.02, 0.76]) for method A and –0.03 mm^2 (95% CI [–0.23, 0.18]) for method B. The authors were therefore able to show that FAF imaging is a reliable imaging modality to assess GA dimensions. Another study[34] verified the intraobserver and interobserver measurement variability of semiautomated software developed for GA lesion size quantification in 30 patients based on confocal FAF imaging. Subjects were recorded at baseline and at 6 and 12 months. At all visits, the GA area was analyzed on central FAF images by seven independent readers using semiautomated software, allowing the direct export of FAF images from the database and semiautomated detection of atrophic areas by shadow correction, vessel detection, and selection of seed points. Mean size of atrophy at baseline was 5.96 mm^2; mean progression rate was 1.25 mm^2/y. Mean difference of interobserver agreement ranged from –0.25 to 0.30 mm^2 for the baseline visit and from –0.14 to 0.11 mm^2/y for the atrophy progression rate. The authors illustrated that FAF provides a reproducible method for quantifying GA and its progression over time.

Intensity-based SD-OCT algorithms for the detection of GA were recently described, enabling its quantification. Yehoshua et al.[35] illustrated a method for identifying GA lesions manually with the use of SD-OCT fundus pseudo-SLO images, applying a digitizing tablet and the appropriate image analysis software. Two graders subsequently outlined the areas of GA identified on the respective OCT fundus image. The encircled area was then quantified using software written in MATLAB, converting the number of pixels into the area of GA. In that study the mean total area at baseline was 4.59 mm^2, and the enlargement rate was 1.2 mm^2 per year. Further, the reproducibility of the method was tested and found to be excellent. The authors therefore found OCT fundus images useful in the visualization and quantification of GA.[35]

Lujan et al.[36] manually compared SD-OCT images with FAF images in patients with GA with respect to lesion size and shape. The authors found that SD-OCT and FAF identified GA reliably and that GA measurements were comparable between the two modalities, with a mean difference of 2.7% of the total area.

While the above-mentioned studies have shown good repeatability of GA lesion quantification by SD-OCT and FAF imaging using manual or semiautomated segmentation, the current study demonstrates good reproducibility of fully automated detection of GA lesion size using the novel PS-OCT technology, capable of specific RPE detection. Automated evaluation of GA lesions by PS-OCT is enabled by the intrinsic tissue-specific polarization contrast (depolarization) of the RPE, a contrast that seems better suited for automatic algorithms than the sometimes rather weak intensity contrast (similar reflectivity of RPE and the photoreceptor-associated boundaries: IS/OS [inner/outer photoreceptor segment boundary] and end tips of photoreceptors). This automated segmentation seems advantageous, as the procedure is fast and does not require the individual expertise of a grader as in labor-intensive and time-consuming manual delineation procedures.

Another advantage of PS-OCT compared to FAF and SLO imaging is the potential of depth-resolved and cross-sectional analysis. PS-OCT allows for specific identification of the presence or absence of the RPE, based on the polarization contrast of backscattered light. Since PS-OCT provides intensity-based OCT images in addition to the capability to detect the RPE in a single instrument, it allows for detailed analysis of the boundaries of the atrophic zone, including irregularities or the identification of foveal involvement. This

Downloaded from iovs.arvojournals.org on 05/07/2021

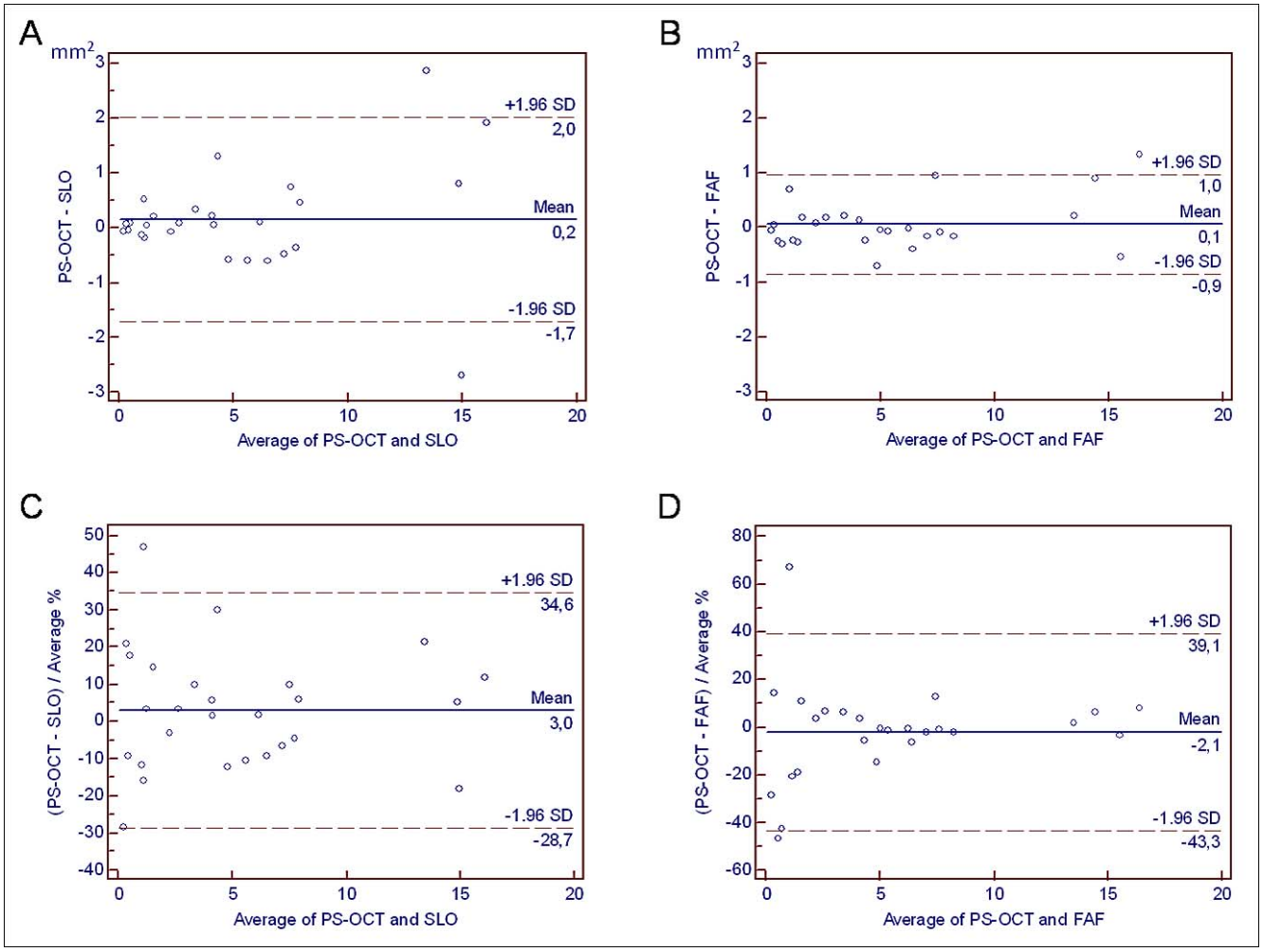

Figure 2. Bland–Altman plots representing PS-OCT results and manually delineated scanning laser ophthalmoscopy (SLO) (**A**, **C**) and autofluorescence (FAF) (**B**, **D**) outcomes of RPE atrophy size measurements (acquired by the Spectralis system). (**A**, **B**) Absolute differences; (**C**, **D**) differences in percentages.

might provide more insight into the reasons some boundaries are stable and others progressively move, leading to GA growth. In particular, the correlation of RPE loss and subsequent atrophy of the overlying neurosensory layer in terms of a selected B-scan representation or as an en face map will provide further insights into the pathophysiology of GA disease and bridge the gap between anatomical and functional alteration.

Regarding automated intensity-based SD-OCT algorithms, the Cirrus HD-OCT Advanced RPE Analysis tool for automatically assessing GA lesion dimensions has been introduced. Further, the automated region finder software for Spectralis in FAF imaging has recently been implemented. We did not use these automated algorithms but used AutoCAD 2008 (Autodesk, San Rafael, CA) for manual delineation purposes, as this program has been successfully used for delineation purposes in GA[37] previously and because the automated algorithms were not available at the time the current study was performed. However, a comparison of the PS-OCT algorithm with these automated SD-OCT–based methods will be considered in future investigations.

Limitations of this study are the relatively low number of patients with multifocal GA and lack of follow-up data. Another shortcoming is the remaining variability of GA lesion size of ~7%, which may be caused by motion artifacts and the lower sampling density in the y direction. Further improvements of the algorithm and high-speed sampling by new complementary metal oxide semiconductor (CMOS) technology[38] might reduce motion artifacts and help to overcome this issue. Another solution to the problem of motion artifacts could be the integration of an eye tracker function, which should be considered in future PS-OCT developments. Although non-foveal residual areas of healthy RPE inside lesions of GA were detected in four patients and were identified reproducibly at identical locations, patients with foveal sparing were not included in this study. This can be considered a weakness of the study and will be analyzed in future investigations.

In conclusion, the current study showed that PS-OCT is applicable in the specific detection of the RPE for reliably quantifying GA lesion size and offers promising perspectives for our understanding of the pathophysiology and disease development. The method is therefore potentially advantageous for the evaluation of therapeutic effects on lesion progression, as currently ongoing studies with a variety of experimental drugs. Automatic lesion size detection will be especially advantageous in large clinical trials once PS-OCT becomes more widely available, for which studies like this are a prerequisite.

Downloaded from iovs.arvojournals.org on 05/07/2021

References

1. Klein R, Klein BE, Knudtson MD, Meuer SM, Swift M, Gangnon RE. Fifteen-year cumulative incidence of age-related macular degeneration: the Beaver Dam Eye Study. *Ophthalmology*. 2007;114:253–262.
2. Wang JJ, Rochtchina E, Lee AJ, et al. Ten-year incidence and progression of age-related maculopathy: the Blue Mountains Eye Study. *Ophthalmology*. 2007;114:92–98.
3. Clemons TE, Rankin MW, McBee WL. Cognitive impairment in the Age-Related Eye Disease Study: AREDS report no. 16. *Arch Ophthalmol*. 2006;124:537–543.
4. Augood CA, Vingerling JR, de Jong PT, et al. Prevalence of age-related maculopathy in older Europeans: the European Eye Study (EUREYE). *Arch Ophthalmol*. 2006;124:529–535.
5. Lim LS, Mitchell P, Seddon JM, Holz FG, Wong TY. Age-related macular degeneration. *Lancet*. 2012;379:1728–1738.
6. Ferris FL III, Fine SL, Hyman L. Age-related macular degeneration and blindness due to neovascular maculopathy. *Arch Ophthalmol*. 1984;102:1640–1642.
7. Hyman LG, Lilienfeld AM, Ferris FL III, Fine SL. Senile macular degeneration: a case-control study. 1983;118:213–227.
8. Klein R, Klein BE, Lee KE, Cruickshanks KJ, Gangnon RE. Changes in visual acuity in a population over a 15-year period: the Beaver Dam Eye Study. *Am J Ophthalmol*. 2006;142:539–549.
9. Sarks JP, Sarks SH, Killingsworth MC. Evolution of geographic atrophy of the retinal pigment epithelium. *Eye (Lond)*. 1988;2:552–557.
10. Augood CA, Vingerling JR, de Jong PT, et al. Prevalence of age-related maculopathy in older Europeans: the European Eye Study (EUREYE). *Arch Ophthalmol*. 2006;124:529–535.
11. de Jong PT. Age-related macular degeneration. *N Engl J Med*. 2006;355:1474–1485.
12. Green WR, Key SN III. Senile macular degeneration: a histopathologic study. *Trans Am Ophthalmol Soc*. 1977;75:180–254.
13. Gass JD. Drusen and disciform macular detachment and degeneration. *Arch Ophthalmol*. 1973;90:206–217.
14. Sarks JP, Sarks SH, Killingsworth MC. Evolution of geographic atrophy of the retinal pigment epithelium. *Eye*. 1988;2:552–557.
15. Maguire P, Vine AK. Geographic atrophy of the retinal pigment epithelium. *Am J Ophthalmol*. 1986;102:621–625.
16. Schatz H, McDonald HR. Atrophic macular degeneration. Rate of spread of geographic atrophy and visual loss. *Ophthalmology*. 1989;96:1541–1551.
17. Sunness JS. The natural history of geographic atrophy, the advanced atrophic form of age-related macular degeneration. *Mol Vis*. 1999;5:25.
18. Klein ML, Ferris FL III, Armstrong J, et al.; AREDS Research Group. Retinal precursors and the development of geographic atrophy in age-related macular degeneration. *Ophthalmology*. 2008;115:1026–1031.
19. Holz FG, Bindewald-Wittich A, Fleckenstein M, et al. Progression of geographic atrophy and impact of fundus autofluorescence patterns in age-related macular degeneration. *Am J Ophthalmol*. 2007;143:463–472.
20. von Ruckmann A, Fitzke FW, Bird AC. Fundus autofluorescence in age-related macular disease imaged with a laser scanning ophthalmoscope. *Invest Ophthalmol Vis Sci*. 1997;38:478–486.
21. Bindewald A, Jorzik JJ, Loesch A, Schutt F, Holz FG. Visualization of retinal pigment epithelial (RPE) cells in vivo using digital high resolution confocal scanning laser ophthalmoscopy. *Am J Ophthalmol*. 2004;137:556–568.
22. Holz FG, Bindewald-Wittich A, Fleckenstein M, Dreyhaupt J, Scholl H, Schmitz-Valckenberg S. Progression of geographic atrophy and impact of fundus autofluorescence patterns in age-related macular degeneration. *Am J Ophthalmol*. 2007;143:463–472.
23. Jorzik JJ, Bindewald A, Dithmar S, Holz FG. Digital simultaneous fluorescein and indocyanine green angiography, autofluorescence, and red-free imaging with a solid-state laser-based confocal scanning laser ophthalmoscope. *Retina*. 2005;25:405–416.
24. Bearelly S, Chau FY, Koreishi A, Stinnett SS, Izatt JA, Toth CA. Spectral domain optical coherence tomography imaging of geographic atrophy margins. *Ophthalmology*. 2009;116:1762–1769.
25. Pircher M, Götzinger E, Leitgeb R, Sattmann H, Findl O, Hitzenberger CK. Imaging of polarization properties of human retina in vivo with phase resolved transversal PS-OCT. *Opt Express*. 2004;12:5940–5951.
26. Götzinger E, Pircher M, Hitzenberger CK. High speed spectral domain polarization sensitive optical coherence tomography of the human retina. *Opt Express*. 2005;13:10217–10229.
27. Pircher M, Götzinger E, Findl O, et al. Human macula investigated in vivo with polarization-sensitive optical coherence tomography. *Invest Ophthalmol Vis Sci*. 2006;47:5487–5494.
28. Ahlers C, Götzinger E, Pircher M, et al. Imaging of the retinal pigment epithelium in age-related macular degeneration using polarization-sensitive optical coherence tomography. *Invest Ophthalmol Vis Sci*. 2010;51:2149–2157.
29. Götzinger E, Pircher M, Geitzenauer W, et al. Retinal pigment epithelium segmentation by polarization sensitive optical coherence tomography. *Opt Express*. 2008;16:16410–16422.
30. Baumann B, Götzinger E, Pircher M, et al. Segmentation and quantification of retinal lesions in age-related macular degeneration using polarization-sensitive optical coherence tomography. *J Biomed Opt*. 2010;15:061704.
31. de Boer JF, Milner TE. Review of polarization sensitive optical coherence tomography and Stokes vector determination. *J Biomed Opt*. 2002;7:359–371.
32. Yamanari M, Lim Y, Makita S, Yasuno Y. Visualization of phase retardation of deep posterior eye by polarization-sensitive swept-source optical coherence tomography with 1-microm probe. *Opt Express*. 2009;17:12385–12396.
33. Schmitz-Valckenberg S, Jorzik J, Unnebrink K, Holz FG; FAM Study Group. Analysis of digital scanning laser ophthalmoscopy fundus autofluorescence images of geographic atrophy in advanced age-related macular degeneration. *Graefes Arch Clin Exp Ophthalmol*. 2002;240:73–78.
34. Schmitz-Valckenberg S, Brinkmann CK, Alten F, et al. Semiautomated image processing method for identification and quantification of geographic atrophy in age-related macular degeneration. *Invest Ophthalmol Vis Sci*. 2011;52:7640–7646.
35. Yehoshua Z, Rosenfeld PJ, Gregori G, et al. Progression of geographic atrophy in age-related macular degeneration imaged with spectral domain optical coherence tomography. *Ophthalmology*. 2011;118:679–686.
36. Lujan BJ, Rosenfeld PJ, Gregori G, et al. Spectral domain optical coherence tomographic imaging of geographic atrophy. *Ophthalmic Surg Lasers Imaging*. 2009;40:96–101.
37. Schütze C, Ahlers C, Sacu S, et al. Performance of OCT segmentation procedures to assess morphology and extension in geographic atrophy. *Acta Ophthalmol*. 2011;89:235–240.
38. Potsaid B, Gorczynska I, Srinivasan VJ, et al. Ultrahigh speed spectral/Fourier domain OCT ophthalmic imaging at 70,000 to 312,500 axial scans per second. *Opt Express*. 2008;16:15149–15169.

Downloaded from iovs.arvojournals.org on 05/07/2021